# In Situ Observation of Changing Crystal Orientations During Austenite Grain Coarsening

**Hemant Sharma, Richard M. Huizenga, Aleksei Bytchkov, Jilt Sietsma and S. Erik Offerman**

**Abstract** Understanding the underlying mechanisms of grain coarsening is important to control the properties of metals, which strongly depend on the microstructure that forms during the production process or use at high temperature. Grain coarsening of austenite at 1,273 K in a binary Fe-2 wt% Mn alloy was studied using synchrotron radiation. The evolution of volume, average crystallographic orientation and mosaicity of more than 2,000 individual austenite grains was tracked during annealing. It was found that there exists an approximately linear relationship between grain size and mosaicity, which means that orientation gradients are present in the grains. The orientation gradients remain constant during coarsening and consequently the character of grain boundaries changes during coarsening, affecting the coarsening rate. Furthermore, changes in the average orientation of grains during coarsening were observed. The changes could be understood by taking the observed orientation gradients and anisotropic movement of grain boundaries into account. Five basic modes of grain coarsening were deduced from the measurements which include: anisotropic (I) and isotropic (II) growth (or shrinkage); movement of grain boundaries resulting in no change in volume but change in shape (III), movement of grain boundaries resulting in no change in volume and mosaicity, but change in crystallographic orientation (IV); and no movement of grain boundaries (V).

**Keywords** In situ · Synchrotron radiation · Iron alloys · Coarsening · Annealing

H. Sharma · R. M. Huizenga · J. Sietsma · S. E. Offerman (✉)
Department of Materials Science and Engineering, Delft University of Technology,
Mekelweg 2, 2628 CD Delft, The Netherlands
e-mail: S.E.Offerman@tudelft.nl

A. Bytchkov
Institute Laue Langevin, BP 156, 38043 Grenoble Cedex, France

# 1 Introduction

This chapter is based on work that we published earlier [1][1]. At high temperatures, coarsening of grains occurs in order to reduce the total energy of the system [2]. Understanding grain coarsening in three-dimensional (3D) structures is essential for control of microstructures of metals and ceramics, which bears a direct influence on the resulting mechanical and functional properties. For example, control of grain size at high temperatures is very important for maintaining high strength of materials over time during operation in energy conversion systems.

For many decades, extensive effort has been devoted to understanding and prediction of grain coarsening at high temperatures. However, even for very simple systems, knowledge of the process of grain coarsening is still incomplete [3, 4]. A substantial part of the work has focused on the development of models for prediction of grain coarsening [4–9]. These models assume grains as perfect crystals, the character of which does not change during coarsening and attribute coarsening entirely to the reduction of total interface area of the system [10], but cannot yet accurately reproduce the real material behavior [2].

Classically grain coarsening at high temperatures in polycrystalline materials is attributed to reduction of the grain boundary area and consequently of the total energy of the system. A widely used semi-empirical grain coarsening equation to fit the experimental data for average grain sizes is expressed as

$$D^n = D_0^n + kt \tag{1}$$

where $D$ is the average grain size at time $t$, $D_0$ is the average grain size at the start of isothermal annealing ($t = 0$) and $k$ and $n$ are empirical fitting parameters [2]. In most studies, values of $n$ are commonly found to be much higher than the ideal value of 2, which is based on proportionality of the local grain curvature driving coarsening and the grain size [2]. A higher value of $n$ means that the rate of grain coarsening decays faster than if $n$ had a lower value. This effect is commonly attributed to solute drag (that is, slowing down of grain boundaries by foreign atoms present in the matrix), to non-regular microstructures or to presence of texture [2], but no underpinning observations for these assumptions have been presented. More recently, a model based on stagnation of grain coarsening induced by grain-boundary smoothening has been proposed [4]. In the present chapter, an additional contribution to the often observed fast decay of the rate of grain coarsening is presented.

Even though significant advances have been made in modeling of coarsening, direct experimental observation of the coarsening process is lacking. Direct experimental observation of grain coarsening at high temperature requires a combination of experimental settings that, until recently, had not been accomplished: in situ observations of *three-dimensional* grain volumes in the bulk of the

---

[1] Reprinted with modification from Acta Materialia, vol. 60, Sharma H, Huizenga RM, Bytchkov A, Sietsma J, Offerman SE, Observation of changing crystal orientations during grain coarsening, pp. 229-237 (2012), with permission from Elsevier.

material during coarsening. Up to date, experimental studies have been limited to ex situ observations on cross-sections of quenched materials [11] or in situ observations on the surface of specimens at high temperature [12]. In the first approach, the time resolution and the accuracy of the observations was limited, especially if the microstructure (e.g. austenite in steel) underwent a phase transformation upon cooling. In the latter case, coarsening at the surface was studied, which can essentially differ from the bulk behavior [13]. In either case, just a 2D analysis of the grain-size distribution was performed.

The recent advances made at 3rd generation synchrotron sources capable of generating high energy X-rays with increased flux have made it possible to observe the bulk of materials [14] and study individual grains in polycrystals [15–19]. In a promising study, Schmidt et al. [20] studied grain coarsening in an aluminum alloy by employing the 3DXRD technique [21]. However, in the case of alloys which undergo a phase transformation upon cooling to room temperature, the technique of interrupted heat treatments as followed by Schmidt et al. [20] cannot be used. In the present chapter, the first in situ three-dimensional observations of bulk grain coarsening at high temperatures in an alloy that undergoes a phase transformation upon cooling are presented. It will be shown that experimental observations at the level of individual grains reveal essential information about the behavior of grains during coarsening.

## 2 Experimental Details

### 2.1 Sample

The alloy under investigation was manufactured from electrolytic (99.999 % purity) iron and manganese to get a composition of 2 wt% Mn. The concentration of other impurities was kept very low in order to minimize any influence of other solute particles on the rate of grain coarsening. The composition was chosen in order to slow down the rate of grain coarsening by solute drag as compared to pure iron. This was warranted by time resolution of the 3DXRD technique used. The initial material was homogenized at 1,553 K for 21 days followed by furnace cooling to room temperature. The sample was manufactured using electro discharge machining (EDM) with dimensions shown in Fig. 1 in order to fit in the furnace described in reference [22]. The sample had a change in diameter from 1 to 1.5 mm in the middle which is used to define a reference by scanning with the X-ray beam.

### 2.2 3DXRD Experiment

The experiment was carried out at beamline ID11 of European Synchrotron Radiation Facility (ESRF), Grenoble, France. Figure 2 shows the experimental setup. The sample was placed in a furnace developed especially for 3DXRD

**Fig. 1** Schematic geometry of the sample. Location of the X-ray beam is highlighted
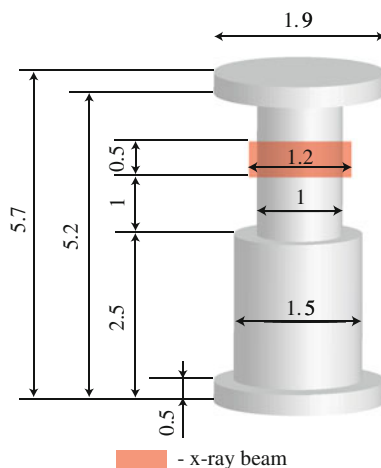


Note: All dimensions are inn mm.

measurements, described in reference [22]. An S-type thermocouple was spot-welded to the top of the sample for accurate temperature control. The sample chamber was purged with helium and sealed at a pressure of 0.4 atm. The X-ray beam, 500 μm high and 1,200 μm wide with energy equal to 88.005 keV, calibrated using a Pb-foil, was incident on the sample at the location depicted in Fig. 1. The sample was heated rapidly to a temperature of 873 K in 60 s, followed by isothermal holding for 900 s and heating to a temperature of 1,173 K at a rate of 0.033 K/s, followed by rapid heating in 120 s to 1,273 K. The sample was then held isothermally at 1,273 K for 7,740 s (2.15 h). During the heat treatment, the furnace was rotated repeatedly over a total angle $\omega$ equal to 24° (so-called *sweep* equal to one full rotation of 24°). Diffraction patterns were recorded during every 0.3° rotation with an exposure time of 0.2 s. This setup means that every 180 s a diffraction pattern is recorded at the same orientation of the sample with respect to the incident beam. The sample was then cooled to room temperature. Due to the limited number of grains in the illuminated volume which satisfy the Bragg condition for diffraction in a certain orientation of the sample, individual spots from individual grains were observed in the diffraction patterns. An example of a diffraction pattern is shown in Fig. 3. The sample to detector distance was adjusted in such a way that four complete diffraction rings of the austenite phase were recorded. An austenite grain of any crystallographic orientation combined with a rotation of the sample over 24° for the first four families of *hkl*-planes would come into diffraction between 3 and 9 times. Thus, all the grains in the illuminated volume were studied in the present experiment. The small rotation angle of 24° means that spatial characteristics of the grains cannot be determined. However, this angle was chosen in order to get a good time resolution. At the beginning and end of isothermal annealing, the vertical size of the X-ray beam was increased to 600 μm in order to verify the diffraction spots originating from the grains situated partially in the illuminated volume.

# 3 Data Analysis Method

This section describes the method that we used to analyze the diffraction patterns. A more extensive description of the methodology is given in two papers by Sharma et al. [23, 24].

## 3.1 Grain Volume

The grain volume is calculated from the diffraction patterns according to the following procedure:

1. The recorded diffraction images are corrected for beam current, electronic noise and detector imperfections.
2. A minimum intensity (threshold) is set in order to identify different peaks originating from grains. In the current case, the threshold is set at 200 counts above the background, which corresponds to a minimum detectable grain volume of around 35 $\mu m^3$ (grain radius of $\sim 2 \, \mu m$). The pixels in the diffraction image which have intensity above the threshold and are connected are identified as a single peak and the sum of intensity of all the connected pixels is stored as integrated intensity from that peak.
3. If the diffraction spot is present in multiple diffraction patterns, that is, if the location of some pixels constituting two or more peaks is the same in the images, the total intensity of the diffraction spot is calculated by summing all the individual peaks and is counted as one diffraction spot.
4. By calibrating the distance between the sample and the detector, all the peaks found in the previous step are assigned to families of *hkl* planes. For this purpose, Transformation code is used, which is a part of the Fable package [25].
5. The location of the center of mass of the diffraction spot is calculated in terms of $\eta$, $2\theta$ and $\omega$ (see Fig. 2 for definitions).
6. The powder intensity ($I_p$) per diffraction image for a *hkl*-ring is calculated by summing the total intensity of all the peaks recorded during one full rotation of the sample (or furnace) over the angle of 24° lying on the *hkl*-ring and dividing by the number of diffraction images. Such a procedure ensures the most accurate value for $I_p$, compensating for texture effects.
7. The volume of the grain ($V_g$) giving rise to the diffraction spot is calculated according to the following expression

$$V_g = \frac{1}{2} m_{hkl} \cos(\theta) V_{gauge} \frac{I_g}{k I_p} \Delta\theta \tag{2}$$

where $m_{hkl}$ is the multiplicity of the *hkl*-ring, $\theta$ is the Bragg diffraction angle, $V_{gauge}$ is the volume of the sample illuminated by the X-ray beam, $I_g$ is the integrated of the diffraction spot, $k$ is the normalization factor for $I_g$ and is
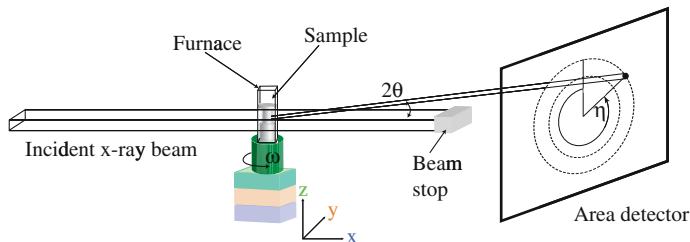
**Fig. 2** Schematic showing the experimental setup. The dimensions are not to scale. The angles $2\theta$, $\omega$ and $\eta$ are defined
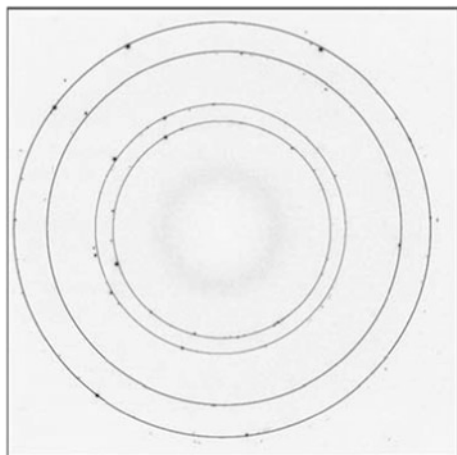


**Fig. 3** Example of a diffraction pattern showing austenite reflections at 1,273 K. Dark regions show pixels with positive intensity. The solid rings indicate the expected location of Debye-Scherrer rings for austenite phase at 1,273 K for the following *hkl* planes (radially outwards): {111}, {200}, {220} and {311}. The deviation of diffraction spots from the ideal location at the diffraction rings is due to the effect of positioning of the diffracting grain inside the sample

equal to the number of diffraction patterns in which the diffraction spot is observed, $I_p$ is the powder intensity per diffraction image for the *hkl*-ring and $D\theta$ is the rotation of plane normal over which the diffraction spot is observed or, in other words, $D\theta$ is the change in the scattering angle due to rotation over $D\omega$. $D\theta$ is given by the following expression

$$\Delta\theta = \sin^{-1}(\sin(\theta)\cos(\Delta\omega) + \cos(\theta)\sin|\eta|\sin(\Delta\omega)) - \theta \qquad (3)$$

where $D\omega$ is the rotation angle of the sample over which the diffraction spot is observed, $\theta$ and $\eta$ are defined in Fig. 2.

For derivation of Eq. (1) and details on Eq. (2), please see the Appendix.

8. The set of volumes obtained during each repeated rotation of the furnace over 24°, from now on called a sweep, are stored as the volumes of austenite grains during that particular sweep in the illuminated volume.

### 3.1.1 Volume Evolution of Individual Grains

1. The volume grains and location of the center of masses of the corresponding diffraction spots are calculated in the previous step. The location of the center of mass of each diffraction spot in a sweep is then matched with the location of the center of masses of all the diffraction spots in the next sweeps.
2. By using a relatively small tolerance ($\pm 3$ pixels in the position of the spot on the detector and $\pm 0.3°$ in $\omega$), the diffraction spots coming from the same grain are identified in different sweeps and the volume of the grain as a function of the time of acquisition of the diffraction pattern is stored.
3. If two or more diffraction spots come from the same austenite grain, the evolution of grain volume must be the same for all of them. By matching the time evolution of grain volumes for all the diffraction spots found with a tolerance of 5 % in volume, a list is generated with the spots belonging to the individual austenite grains. The total volume of the grains found in such a manner is 97.3 % of the illuminated volume, the rest being grains for which the diffraction spots overlap or grains which are too small to be detected.
4. The volume of the grain is taken to be the average of the volumes resulting from all the diffraction spots belonging to the same grain per sweep.
5. The spots which show an increase in intensity more than 5 % of the integrated intensity upon opening of the X-ray beam are rejected as coming from the grains which are partially illuminated by the X-ray beam.
6. The number of grains during each sweep is calculated by counting the total number of grains identified in step 3.
7. The average austenite grain volume of all the austenite grains is calculated by computing the volume weighted average of the grain volumes.

### 3.1.2 Calculation of Mosaicity of the Grains

Mosaicity, $\Delta \upsilon$, defined per grain as the maximum difference in crystallographic orientation between any two regions in the grain [26], was calculated as the rotation of the diffracting plane normal required to produce a diffraction spot of the observed size in $\omega$ and $\eta$. In either $\omega$ or $\eta$, the mosaicity calculated is the maximum difference in orientation in a single direction of the grain. The average mosaicity was calculated as the average mosaicity of all the grains with radius between intervals of

5 μm.[2] The mosaicity per grain was calculated by averaging the mosaicity calculated from all the diffraction spots identified as belonging to the grain.[3]

The following procedure was used to calculate the mosaicity:

1. The mosaicity or the maximum difference in orientation of plane normal between any two regions of the grain can be characterized by analyzing the diffraction spots arising from the grain.
2. In case of an un-deformed grain, the change in orientation of a grain with an isotropic shape is assumed to be isotropic in all directions.
3. In diffraction, the mosaicity of a grain can be described in terms of the size of the diffraction cloud in reciprocal space. The size of a diffraction spot on the detector is the convolution of the beam divergence, the Darwin width of the reflection, the size of the diffracting grain and the mosaicity of the grain. In the current experimental setup, the location of the detector far away from the sample (375 mm) and use of an undulator beamline at a synchrotron mean that the size of the grain and the divergence of the X-ray beam have a negligible effect on the size of the spot as compared to the mosaicity of the grain. Furthermore, the Darwin width of the reflection, which can also cause widening of the spot, has a negligible contribution in the current experimental setup.
4. In terms of the diffraction geometry shown in Fig. 2, the mosaicity of the grain can be calculated either by calculating the size of spot ($\Delta\eta$) along the $\eta$-direction (mosaicity by rotation of the diffracting plane normal around the X-ray beam) or the rotation of plane normal, $\Delta\theta$ (mosaicity by rotation around the diffraction plane normal) from Eq. (3), characterizing the diffraction spot. Depending on the number of diffraction patterns that the diffraction spot is present in, the following strategy is used to calculate the mosaicity of the austenite grains:

   (a) If the diffraction spot is present in one or two diffraction patterns, the mosaicity of the grain from the diffraction spot is calculated by calculating the rotation of the plane normal corresponding to the size of the diffraction spot in $\eta$-direction corrected for the divergence of the X-ray beam which is known from the setup. In this method, the error in characterizing the mosaicity is equal to the effect of the size of the grain.
   (b) If the diffraction spot is present in three or more diffraction patterns, the mosaicity of the grain is calculated by calculating the spread of the diffraction spot in $\omega$-direction. The amount of rotation in $\omega$ for which the grain is in diffraction is calculated as follows:

---

[2] In case of very big grains diffraction spots in first and second diffraction rings are saturated and thus cannot be used for analysis. In such cases, spots from third and fourth rings were used for calculating the mosaicity. However, this has the disadvantage that mosaicity of such grains is underestimated arising from problems with the background. Due to this reason, average mosaicity was calculated only for grains with radiuses up to 130 μm.

[3] In this way, the mosaicity calculated is the average of maximum orientation difference in multiple directions. This was done in order to compare the mosaicity with equivalent grain radius.

$$\Delta\omega = \omega_{step}\left(\frac{I_1}{I_2} + (n-2) + \frac{I_n}{I_{n-1}}\right) \qquad \text{(S(iii))}$$

where $\omega_{step}$ is the rotation step during acquisition of each diffraction pattern, $n$ is the number of diffraction patterns in which the diffraction spot is present, $I_n$ is the intensity of the diffraction spot in the $n$-th diffraction pattern.

Equation S(iii) takes into account the fact that the grain is not in diffraction for the whole $\omega_{step}$ in the first and the last diffraction pattern. The mosaicity of the grain from the diffraction spot is then equal to the rotation of plane normal, $\Delta\theta$, calculated from Eq. S(ii). In this method, the maximum error in characterizing the mosaicity is equal to the value of $\Delta\theta$ corresponding to half the value of $\omega_{step}$.

5. The value of mosaicity of the grain, calculated by the procedure mentioned above, is always in only one direction in the grain. In reality, however, the mosaicity can be slightly different in different directions. Thus, the average value of mosaicity of the grain is calculated by averaging the mosaicity corresponding to different diffraction spots from the grain.

### 3.1.3 Calculation of Rotation of Average Plane Normal

The average normal to a diffracting plane was calculated using the centre of mass of the diffraction spots belonging to the grain. The rotation of the average plane normal was then calculated by calculating the angle between the average plane normal of the spots for the first and the successive sweeps.

The following procedure was used to calculate the rotation of the average plane normal:

1. The direction of plane normal of a reflection corresponding to the orientation of the center of mass for an austenite grain is calculated by assuming that the center of mass of the grain is present in the center of the sample and in the center of the beam. This assumption does not give any error for the present calculation if the center of mass of the grain does not move more than 100 μm during coarsening.
2. The center of mass of the diffraction spot is used to calculate the direction of the average plane normal.
3. The rotation of the average plane normal is calculated by calculating the angle between the average plane normal of the grain for the first and the successive sweeps.
4. The value of rotation of the average plane normal is then calculated by averaging the rotations per sweep calculated from different diffraction spots from the same grain.
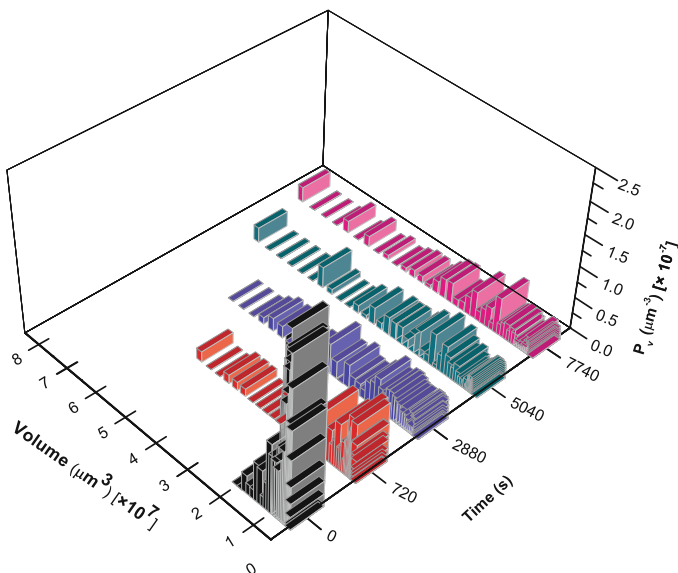
**Fig. 4** Evolution of austenite grain size distribution ($P_v$) during isothermal annealing at 1,273 K

## 4 Results

Figure 4 shows the evolution of the volume-weighted-grain-size distribution ($P_v$) in the sample as a function of isothermal annealing time. It can be seen that, consistent with the general idea of grain coarsening, the fraction of the illuminated volume occupied by small grains is high in the beginning of isothermal annealing which gradually decreases as the coarsening progresses. This is reflected in Fig. 5, where the volume-averaged grain volume (red symbols) and the number of grains in the illuminated volume (black symbols) as a function of annealing time are shown. It can be seen that as coarsening progresses, the average grain volume increases and the number of grains in the illuminated volume decreases.

The average volume of austenite grains (Fig. 5, red symbols) increased from $1.24 \times 10^6$ $\mu m^3$ at $t = 0$ s to $9.08 \times 10^6$ $\mu m^3$ at $t = 7,740$ s. The best fit (Fig. 5, blue curve) of the average austenite grain size data to Eq. (1) gives value of the grain coarsening exponent $n = 8.3$. This value is much higher than the reference value of 2, an observation made more often in literature [2]. During annealing, the number of grains in the illuminated volume decreased from 2,385 at $t = 0$ s to 1,201 at $t = 7,740$ s (Fig. 5, black symbols). Out of the 2,385 initial grains, 104 grains increased in volume, 283 had an eventual change in volume less than 5 %, 814 grains decreased in volume by more than 5 % and 1,184 grains disappeared completely.

To highlight the relationship between size and mosaicity of grains, the average mosaicity for all the grains in the illuminated volume is plotted in Fig. 6 as a
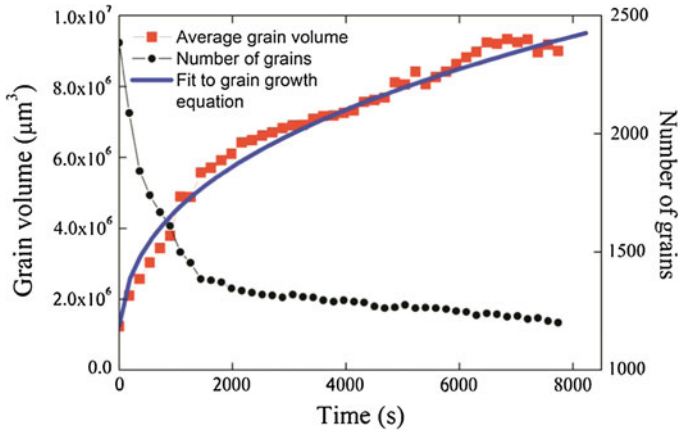
**Fig. 5** Grain characteristics during isothermal annealing at 1,273 K. Evolution of number of grains in the illuminated volume as a function of annealing time (*black circles*) and evolution of volume-averaged grain volume as a function of annealing time (*red squares*). The *blue curve* shows the best fit to Eq. (1)

**Fig. 6** Plot of the average mosaicity of all the grains during isothermal annealing as a function of grain radius
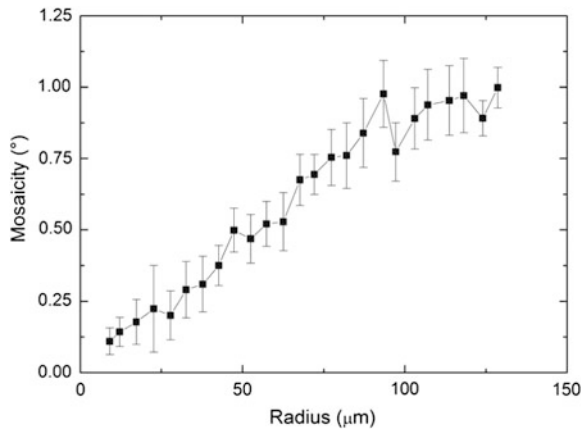


function of the equivalent grain radius (calculated from grain volume by assuming spherical grain shape). The error bars for the average mosaicity give the standard deviation of the observed mosaicity among the observed grains. Figure 6 shows that there exists an approximately linear relationship between mosaicity and grain radius.

For five austenite grains out of the 2,385 observed grains, Fig. 7 shows the evolution of grain volume, mosaicity and rotation of the average plane normal. It can be seen that, in comparison to the average grain coarsening behavior shown in Fig. 5 (red symbols), the volume evolution of individual austenite grains varies considerably. Figure 7a shows an example of an austenite grain that grows continuously over time. The evolution of the grain is similar to the average grain
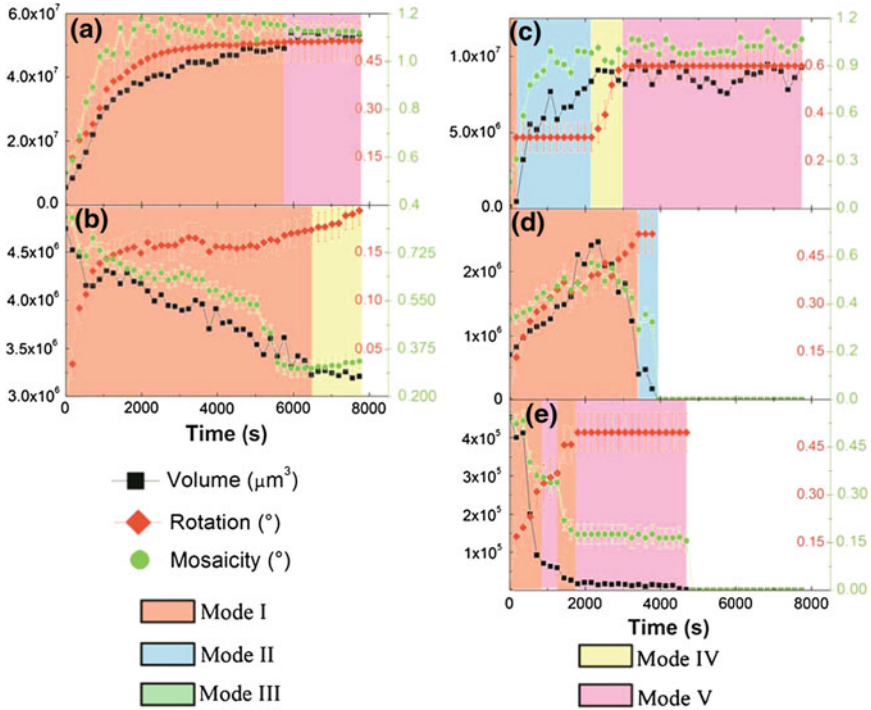
**Fig. 7** Evolution of grain volume (*black squares*), cumulative rotation of average plane normal with respect to the original orientation (*red diamonds*) and change in mosaicity (*green circles*) of individual austenite grains during isothermal annealing at 1,273 K. Different shading colors represent regions of different modes shown in Fig. 8. **a** Example of an austenite grain which increases in size. **b** An austenite grain shrinking continuously over time. **c** Example of an austenite grain which grows first and then has constant volume. **d** Example of a grain which initially grows and then shrinks to disappear. **e** Example of a grain which decreases in volume, becomes stable and then shrinks to disappear. The error bars are calculated based on the error in measurement of the quantity

coarsening behavior shown in Fig. 5. However, the grains shown in Fig. 7b–e exhibit a combination of evolution of size of the grains completely different from the evolution of the average grain size in Fig. 5. The grain in Fig. 7b shrinks continuously; the grain in Fig. 7c witnesses rapid growth and then stabilizes in volume; the grain in Fig. 7d first grows, followed by shrinkage, and then disappears; and the grain in Fig. 7e shrinks, stabilizes in volume and then disappears.

A crucial feature of Fig. 7a is the development of mosaicity of the grain, which follows evolution of volume of the growing grain. This is consistent with the results for average mosaicity of all the grains shown in Fig. 6. The grains shown in Fig. 7b–e exhibit the same behavior, that is, the mosaicity of a grain follows the evolution of its volume. This shows that the direct relationship between mosaicity and size of the grains is also maintained during coarsening. Furthermore, Fig. 7a–e

show that the average orientation of diffracting plane normal for the grains changes during coarsening. The information shown in Figs. 6 and 7 is unique in terms of the extended insight that can be obtained into the behavior of individual grains during coarsening.

## 5 Discussion

It is shown in Figs. 6 and 7 that the mosaicity of a grain is directly proportional to its radius and that this relationship holds true during coarsening. The direct relationship between grain mosaicity and radius implies that crystallographic orientation gradients exist in the grains, which persist during coarsening such that during growth of a grain the variations in its orientation increase. The presence of orientation spreads in well-annealed grains has been observed before in literature [27], but the present measurements of constant orientation gradients in grains during coarsening are first of their kind. This is very interesting, since even though, from a theoretical viewpoint, the presence of variations in orientations of crystals is thermodynamically unfavorable [2], the present observations show that not only are crystallographic orientation gradients present in the grains, but also that their magnitude does not reduce during coarsening, but remains constant instead.

Based on the observation of maintenance of constant orientation gradients, a total of five different modes of grain evolution (shown in Fig. 8 and Table 1) can occur:

1. Mode I—anisotropic growth, I(a), or shrinkage, I(b), leads to an increase in the total mosaicity of the grain and a change in the average orientation.
2. Mode II—isotropic growth, II(a), or shrinkage, II(b), leads to increase in total mosaicity but the average orientation remains constant.
3. Mode III—combination of anisotropic growth and shrinkage result in the same volume, however, the mosaicity increases in one direction while it decreases in another direction. The average orientation changes after annealing in mode III(a). Another variant, mode III(b), of this mode is when the average orientation of the grain remains constant while the mosaicity in different direction changes.
4. Mode IV—combination of anisotropic growth and shrinkage results in the same volume and mosaicity of the grain, whereas the average orientation changes after annealing.
5. Mode V—no movement of grain boundaries occurs. Volume, mosaicity and average orientation of the grain remain constant.

The case of shrinkage is analogous to growth and additional features of each mode are explained in Table 1. Different shading colours in Fig. 7 are used to highlight the mode of evolution of the grains in different periods during annealing. An interesting case is the grain shown in Fig. 9, the volume of which remains constant during annealing but the grain exhibits a combination of Mode III (which

**Fig. 8** Schematic illustration
of the possible effects of grain
evolution on mosaicity and
average orientation of the
austenite grains for the
simplified case of grains
having a constant orientation
gradient in radial direction.
Colors represent orientation.
The cases of shrinkage are
analogous to growth



I

II

Initial grain

III

V

IV

······ - Initial grain position

⊙ - Initial average orientation
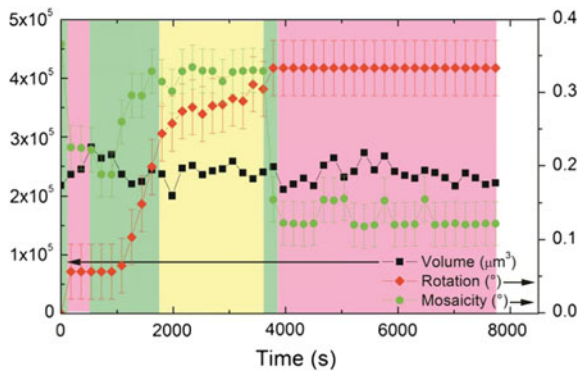
● - Final average orientation
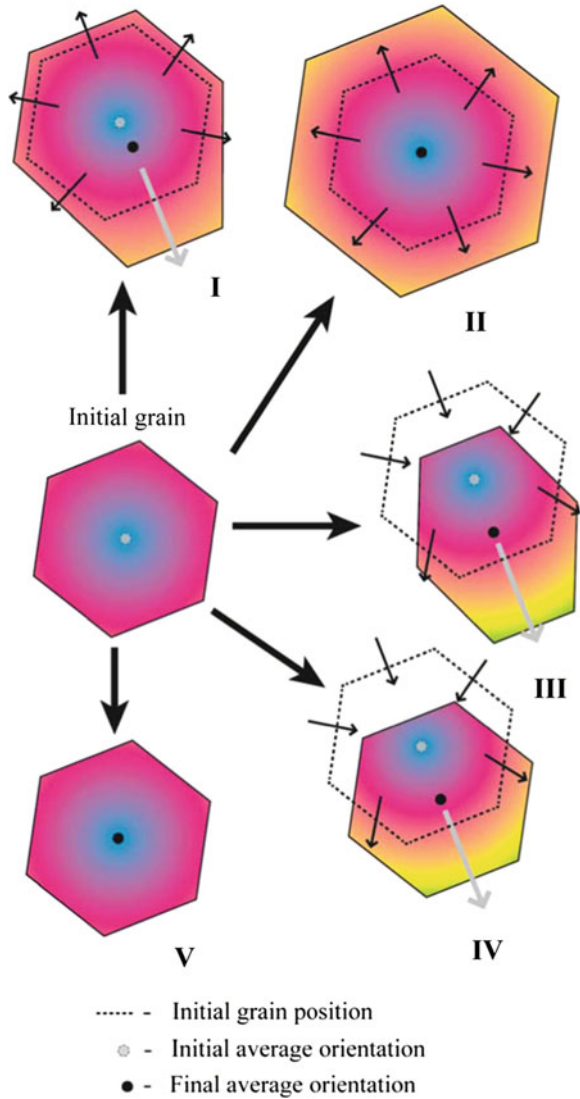
indicates changes in shape), Mode IV (which indicates no change in shape but change in centre-of-mass position) and Mode V (which indicates no apparent grain boundary movement). In order to highlight shape effects, mosaicity of the grain in Fig. 9 is calculated using a single diffraction spot such that mosaicity in only one direction is measured. Even though the total volume of the grain remains constant, local grain boundary motion combined with constant orientation gradients can lead to changes in mosaicity and average orientation as seen in Fig. 9.

**Table 1** Features of the different modes of evolution of grains shown in Fig. 9

| Mode no. | Volume | Rotation of average plane normal | Mosaicity |
|----------|--------|----------------------------------|-----------|
| I(a) | + | Δ | + |
| I(b) | − | Δ | − |
| II(a) | + | = | + |
| II(b) | − | = | − |
| III(a) | = | Δ | ± |
| III(b) | = | = | ± |
| IV | = | Δ | = |
| V | = | = | = |

The corresponding change in grain volume, rotation of the average plane normal and mosaicity is listed. For rotation of the plane normal, there is no distinction between + or − and change is indicated by Δ. For mosaicity, ± means increase in one direction and decrease in another direction



**Fig. 9** Example of evolution of grain volume (*black squares*), cumulative rotation of average plane normal with respect to the original orientation (*red diamonds*) and change in total mosaicity (*green circles*) of an austenite grain with constant volume. The axis on *left* is for volume of the grain and the axis on *right* is for the rotation of the diffracting plane normal and the mosaicity of the grain. Different shading colors (legend in Fig. 7) represent regions of different modes shown in Fig. 8

In literature, it has been proposed by the use of simulations that grains in nano-crystalline size range can rotate during coarsening [28, 29], similar to the observed change in orientation of the average diffracting plane normal for the grains in Fig. 7. However, the grains shown in Fig. 6 are of a much bigger size (of the order of tens to hundreds of μm in radius) and rotation of the whole volume of these large grains during coarsening in absence of external stresses is not expected. The constant orientation gradients in grains can be considered to explain the observed changes in average diffracting plane normal. The average orientation of a grain, if the observed constant gradients in orientation are present, is essentially the orientation of centre of mass of the grain. Thus, in case of anisotropic growth (or shrinkage) of grains, when centre of mass of the grains shifts, the average
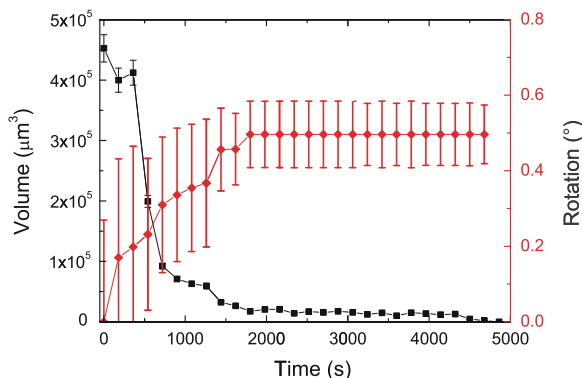
**Fig. 10** Example of an austenite grain, same as in Fig. 7e, for which orientation in the beginning of isothermal annealing is completely different from orientation just before disappearing. Evolution of grain volume is shown by *black squares* and cumulative rotation of the average diffracting plane normal with respect to the original orientation is shown by *red diamonds*. The error bars of rotation of the average diffracting plane normal are equal to the mosaicity of the grain

orientation of grains changes as well. An extreme case is for the grain in Fig. 6e shown in Fig. 10, where the error bars of rotation of the average diffracting plane normal are equal to the mosaicity of the grain and thus the limits of the error bars represent the extrema of orientation in the grain. The observed change in average orientation and the reduction in mosaicity mean that no part of the grain remaining at 4,000 s has the same orientation as any part of the grain which was present at the start of isothermal annealing. This is particularly interesting, since, in case of an ex situ study, if the same grain was observed at the beginning of annealing and at 4,000 s into annealing, the different orientations would suggest that a new grain had nucleated.

Having established that grains at high temperatures have orientation gradients which remain constant during coarsening, the possible implications of the results on the process of grain coarsening are now examined. Even though the presence of orientation spreads in grains is well known [2, 3, 27], their influence on the process of coarsening has not been explored before.

Grain coarsening at high temperatures in polycrystalline materials occurs in order to reduce the total interface energy of the system ($\int \gamma dA$, with $\gamma$ the specific interfacial energy and the integration running over the grain boundary area in the microstructure). For each grain boundary, its contribution to the total interface energy of the system can be reduced either by reducing the contributing interface area, $A$, or the specific interface energy, $\gamma$. Reduction in $A$ takes place by increase of the radius of curvature of the grain boundaries, so-called capillarity-driven grain coarsening [2]. It has been proposed before by means of simulations that $\gamma$ can be reduced by changes in the inclination of the grain boundaries [30]. The average interface energy can also be reduced by direct elimination of high energy grain boundaries during grain coarsening [10].

The present observations show that orientation gradients are present in grains and that these gradients remain constant during coarsening. This means that, in the case of neighbouring grains, both having an orientation gradient, the movement of a grain boundary combined with observed constant orientation gradient in all regions of the grains would change the local misorientation (difference in orientation at opposite sides of the grain boundary) across the grain boundary. This can be expected to affect the specific grain-boundary energy ($\gamma$), since it is known that $\gamma$ depends on the misorientation angle ($\theta$) between the grains constituting the grain boundary [3]. In simple terms, the relation between change in interface energy ($\Delta\gamma$) and the change in misorientation ($\Delta\theta$) can be written as:

$$\Delta\gamma = \left(\frac{\partial\gamma}{\partial\theta}\right)\Delta\theta \qquad (4)$$

Depending on the sign and magnitude of ($\partial\gamma/\partial\theta$), Eq. (4) can result in three cases: $\Delta\gamma = 0$, $\Delta\gamma < 0$ and $\Delta\gamma > 0$. In case $\Delta\gamma = 0$, there would be no effect on the driving force for grain coarsening, $G$, and grain coarsening would be driven only by curvature. In cases when $\Delta\gamma$ is negative, for example in the case of low-angle grain boundaries with decreasing $\Delta\theta$, this would result in a decrease in $G$, since $G$ is directly proportional to $\gamma$. This results, in turn, in additional decay of the rate of grain coarsening during the process. The motion of the grain boundary in this fashion would continue with an ever decreasing rate until the grain boundary reaches a minimum in $\gamma$. In cases where $\Delta\gamma$ is positive, the motion of the grain boundary would lead to an increase in $\gamma$. Even though $\gamma$ increases, the total interface energy contribution of the grain boundary, $\int \gamma dA$, could still continue to decrease as long as the decrease in the interface area, $A$, can compensate for the increase in $\gamma$. A meta-stable condition would be reached when the motion of the grain boundary in any direction leads to an increase in $\int \gamma dA$, either by increasing $A$ or $\gamma$. Thus, for materials with a distribution of grain boundaries of multiple characters, the combined effect of the latter two cases would be a reduction in the overall rate of grain coarsening and increase in the grain coarsening exponent, $n$. It must be noted here that in situ experimental measurement of $\gamma$ during coarsening is not possible with the techniques presently available.

The next step is to examine the probability of occurrence of the two cases which affect $n$. The change in misorientation due to movement of grain boundaries and the added imposition of maintenance of the orientation gradient will be of the order of a degree. This means that the grain boundaries, the energy of which is strongly dependent on the misorientation, for example, low angle tilt boundaries or special $\sum$ boundaries, are affected strongly by the relatively small change in misorientation. It is already known that the fraction of these special low energy grain boundaries in materials is high and increases during annealing [10, 31, 32]. Thus, always a high fraction of grain boundaries in materials would be affected by the change in misorientation resulting from maintenance of a constant orientation gradient.

# 6 Conclusions

Grain coarsening of austenite in a binary Fe-2 wt% Mn alloy was studied by measuring the evolution of volume, average crystallographic orientation and mosaicity of more than 2,000 individual austenite grains during annealing at 1,273 K. The following conclusions can be drawn from the measurements:

1. For more than 2,000 austenite grains, it was observed that the average mosaicity of all the grains is approximately directly proportional to the average grain size of the grains.
2. For individual grains, it is shown that mosaicity is directly proportional to the grain volume at all times during coarsening at 1,273 K. This means that constant orientation gradients exist in the grains which persist during coarsening.
3. The persistence of orientation gradients coupled with movement of grain boundaries results in changes in the grain boundary character, affecting the coarsening rate.
4. Changes in the average orientation of large (10–200 μm in radius) austenite grains were observed during coarsening.
5. Five modes of grain growth are proposed: anisotropic (I) and isotropic (II) growth (or shrinkage); movement of grain boundaries resulting in no change in volume but change in shape (III) and movement of grain boundaries resulting in no change in volume and mosaicity, but in the average crystallographic orientation (IV); and no movement of grain boundaries (V).

# A.1 7   Appendix

## A.1.1  Equation of Volume of a Grain

The diffracted intensity $I_g$ per unit time from a single grain, rotated through the Bragg condition in order to illuminate the whole grain, is given by the following expression for the kinematic approximation (4, 5):

$$I_{grain} = \frac{I_0}{\Delta\theta}\left(\frac{\mu_0}{4\pi}\right)^2\frac{e^4}{m^2}\frac{\lambda^3 F_{hkl}^2}{V_c^2}V_g L_g P\exp(-2M) \qquad (S(vi))$$

where $I_0$ is the incident intensity of photons, $F_{hkl}$ is the structure factor of the *hkl*-reflection, $\lambda$ is the photon wavelength, $V_g$ is the volume of the grain, $\Delta\theta$ is the

change in scattering vector over which the grain is in reflection (Eq. S(ii)), $V_c$ is the volume of the unit cell, $P = (1 + \cos^2 2\theta)/2$ is the polarization factor, and $L_g = 1/\sin 2\theta$ is the Lorentz factor, where $2\theta$ is the scattering angle. The Debye-Waller factor $\exp(-2M)$ accounts for the thermal vibrations of atoms, with

$$M = \frac{6h^2 T}{mk_B \Theta^2}\left[\phi(x) + \frac{x}{4}\right]\left(\frac{\sin\theta}{\lambda}\right)^2 \qquad \text{(S(vii))}$$

where $h$ is the Planck constant, $m$ is the mass of the vibrating atom, $k_B$ is the Boltzmann constant, $\Theta$ is the Debye temperature, $x = \Theta/T$ is the relative temperature, $T$ is the temperature and

$$\phi(x) = \frac{1}{x}\int_0^x \frac{\xi}{\exp(\xi) - 1} d\xi \qquad \text{(S(viii))}$$

The integrated intensity $I_p$ per unit time of a $hkl$-diffraction ring of a polycrystalline material (often termed as powder in diffraction) with randomly oriented grains is given by (4, 5)

$$I_{powder} = \Phi_0 \left(\frac{\mu_0}{4\pi}\right)^2 \frac{e^4}{m^2} \frac{\lambda^3 m_{hkl} F_{hkl}^2}{V_c^2} V_{gauge} L_p P \exp(-2M) \qquad \text{(S(ix))}$$

where $m_{hkl}$ is the multiplicity factor of the $hkl$-ring and $V_{gauge}$ is the volume of the diffracting phase. The Lorentz factor for a powder is given by $L_p = 1/(4\sin\theta)$.

The volume of an individual grain is calculated from the measured grain intensity $I_g$ normalized by the powder intensity $I_p$ of the $hkl$-ring in which the reflection from the individual grain appeared. In case the diffraction spot appears in more than one diffraction pattern, the intensity from the grain is divided by a factor $k$, equal to the number of diffraction patterns in which the spot is present. Combining Eqs. S(vi)) and S(ix) and introducing $k$ gives Eq. S(i)

$$V_g = \frac{1}{2} m_{hkl} \cos(\theta) V_{gauge} \frac{I_g}{kI_p} \Delta\theta \qquad \text{(S(i))}$$

Equation S(i) is similar to the equation for volume of a grain used by Lauridsen et al. (6) and Offerman et al. (7). However, the following corrections have been made-

1. In the current analysis, diffraction spots distributed in more than one diffraction pattern were used for the volume calculation. Thus, the additional factor $k$ is used.
2. The expression for $\Delta\theta$ used by Lauridsen et al. and Offerman et al. is $\Delta\theta = \Delta\omega \cdot |\sin(\eta)|$. However, this is an approximation which does not hold for low values of $\eta$. In the current analysis, Eq. S(ii) is used which is the exact

form of the expression for $\Delta\theta$. From Fig. S6, the expression for $\Delta\theta$ can be calculated as follows:

The projection along the *x-axis* of the vector $(x, y, z)$ of length $r$ in the direction of the plane normal before rotation is given as

$$x = -r\sin\theta$$

After rotation, the vector is given as

$$x' = -r\sin(\theta + \Delta\theta) \tag{S(x)}$$

Also, applying the rotation transform on vector $r'$ gives

$$x' = -r\sin\theta\cos\Delta\omega - r\sin\eta\sin\Delta\omega\cos\theta \tag{S(xi)}$$

Combining Eqs. S(x) and S(xi) gives Eq. S(ii)

$$\Delta\theta = \sin^{-1}(\sin(\theta)\cos(\Delta\omega) + \cos(\theta)\sin|\eta|\sin(\Delta\omega)) - \theta \tag{S(ii)}$$

# References

1. Sharma H, Huizenga RM, Bytchkov A, Sietsma J, Offerman SE (2012) Observation of changing crystal orientations during grain coarsening. Acta Materialia 60:229–237
2. Humphreys FJ, Hatherly M (2004) Recrystallization and related annealing phenomena. Elsevier, Oxford
3. Gottstein G, Shvindlerman LS (1999) Grain boundary migration in metals: thermodynamics, kinetics, applications. CRC Press, Boca Raton
4. Holm EA, Foiles SM (2010) How grain growth stops: a mechanism for grain-growth stagnation in pure materials. Science 328:1138
5. von Neumann J (1952) Discussion. In: Herring C (ed) Metal interfaces. American Society for Metals, Cleveland, p 108
6. Hillert M (1965) On the theory of normal and abnormal grain growth. Acta Metall 13:227
7. Mullins WW (1989) Estimation of the geometrical rate constant in idealized three dimensional grain growth. Acta Metall 37:2979
8. Glazier JA (1993) Grain growth in three dimensions depends on grain topology. Phys Rev Lett 70:2170
9. MacPherson RD, Srolovitz DJ (2007) The von Neumann relation generalized to coarsening of three-dimensional microstructures. Nature 446:1053
10. Rohrer GS (2005) Influence of interface anisotropy on grain growth and coarsening. Annu Rev Mater Res 35:99
11. Militzer M, Giumelli A, Hawbolt EB, Meadowcroft TR (1996) Austenite grain growth kinetics in Al-killed plain carbon steels. Metall Mater Trans A Phys Metall Mater Sci 27:3399
12. Zhou TH, O'Malley RJ, Zurob HS (2010) Study of grain growth kinetics in delta-ferrite and austenite with application to thin-slab cast direct-rolling microalloyed steels. Metall Mater Trans A Phys Metall Mater Sci 41A:2112

13. Mullins WW (1958) The Effect of Thermal Grooving on Grain Boundary Motion. Acta Metall 6:414
14. Krill CE, Helfen L, Michels D, Natter H, Fitch A, Masson O et al (2001) Size-dependent grain-growth kinetics observed in nanocrystalline Fe. Phys Rev Lett 86:842
15. Margulies L, Winther G, Poulsen HF (2001) In situ measurement of grain rotation during deformation of polycrystals. Science 291:2392
16. Poulsen HF, Nielsen SF, Lauridsen EM, Schmidt S, Suter RM, Lienert U et al (2001) Three-dimensional maps of grain boundaries and the stress state of individual grains in polycrystals and powders. J Appl Crystallogr 34:751
17. Offerman SE, van Dijk NH, Sietsma J, Grigull S, Lauridsen EM, Margulies L et al (2002) Grain nucleation and growth during phase transformations. Science 298:1003
18. Larson BC, Yang W, Ice GE, Budai JD, Tischler JZ (2002) Three-dimensional X-ray structural microscopy with submicrometre resolution. Nature 415:887
19. Schmidt S, Nielsen SF, Gundlach C, Margulies L, Huang X, Jensen DJ (2004) Watching the growth of bulk grains during recrystallization of deformed metals. Science 305:229
20. Schmidt S, Olsen UL, Poulsen HF, Sørensen HO, Lauridsen EM, Margulies L et al (2008) Direct observation of 3-D grain growth in Al–0.1% Mn. Scripta Mater 59:491
21. Poulsen HF (2004) Three-dimensional X-ray diffraction microscopy-mapping polycrystals and their dynamics. Springer, Berlin
22. Sharma H, Wattjes AC, Amirthalingam M, Zuidwijk T, Geerlofs N, Offerman SE (2009) Multipurpose furnace for in situ studies of polycrystalline materials using synchrotron radiation. Rev Sci Instrum 80:7
23. Sharma H, Huizenga RM, Offerman SE (2012) A fast methodology to determine characteristics of large numbers of grains using 3DXRD. I: overlapping diffraction peaks and global parameters. J Appl Crystallogr 45:693–704
24. Sharma H, Huizenga RM, Offerman SE (2012) A fast methodology to determine characteristics of large numbers of grains using 3DXRD. II: volume, centre-of-mass position and crystallographic orientation of grains. J Appl Crystallogr 45:705–718
25. http://sourceforge.net/apps/trac/fable/wiki. Last Accessed 01 Aug 2011
26. Warren BE (1990) X-ray diffraction. Dover Publications, New York
27. Landheer H (2010) Nucleation of ferrite in austenite. PhD thesis. Department of Materials Science and Engineering, Delft University of Technology, Delft
28. Haslam AJ, Phillpot SR, Wolf H, Moldovan D, Gleiter H (2001) Mechanisms of grain growth in nanocrystalline fcc metals by molecular-dynamics simulation. Mater Sci Eng A Str Mater Prop Microstruct Process 318:293
29. Farkas D, Mohanty S, Monk J (2007) Linear Grain Growth Kinetics and Rotation in Nanocrystalline Ni. Phys Rev Lett 98:165502
30. Upmanyu M, Srolovitz DJ, Lobkovsky AE, Warren JA, Carter WC (2006) Simultaneous Grain Boundary Migration and Grain Rotation. Acta Mater 54:1707
31. Watanabe T, Fujii H, Oikawa H, Arai KI (1989) Acta Metall 37:941
32. Holm EA, Hassold GN, Miodownik MA (2001) Acta Mater 49:2981